Supplementary Materials of

Multi-stable origami structures with thick panels

Heming Wang[†]*, Zhuangzhi Miao*[†]*, Tong Zhou, Ke Liu, Haitao Ye, Yang Li*[*]

Contents in this PDF file:

[*]Corresponding author: yang.li@whu.edu.cn
[†]These authors contribute equally to this work.

1 Derivation of structural compatibility conditions in single-vertex MSTO structures

1.1 Parameterization of MSTO structures

There are four hinges in the degree-4 MSTO structure as in Fig. S1(A). From the perspective of D-H notation[41], the MSTO structure could be parameterized by the relative location of these four hinges, which is expressed by kinematic parameters and structural parameters. For MSTO structures only with out-of-plane hinge-shift, the kinematic parameters are the rotation angle θ_i of hinge h_i, the structural parameters include the out-of-plane hinge shifting distance d_i for the hinge, and the pattern angle $\alpha_{i,j}$, which is the angle from hinge H_i to hinge H_j. For MSTO structures with out-of-plane and in-plane hinge shifting, the additional structural parameter is the in-plane hinge shifting distance d_i as in Fig. S1(B). Similarly to MSTO structures additionally with hinge inclination, the new-introduced structural parameters is the inclination angle β_{ij} as in Fig. S1(C).

1.2 Degree-4 MSTO structure without in-plane hinge-shift

For the MSTO structure without the in-plane hinge-shift technique, the translation relation among the rotational hinges can be expressed by the rotation along the x-axis and z-axis in the hinges' coordinate system and the translation along the z-axis. Therefore, the transformation between the adjacent hinges can be expressed by the multiplication of the rotation and translation matrixes, as shown in the following equation:

$$Q_{ij}(\theta_{ij}, \alpha_{ij}, h_{ij}) = R_z(\theta_{ij})T_x(h_{ij})R_x(\alpha_{ij}), \tag{1}$$

where

$$R_x(\alpha_{ij}) = \begin{bmatrix} 1 & 0 & 0 & 0 \\ 0 & \cos(\alpha_{ij}) & -\sin(\alpha_{ij}) & 0 \\ 0 & \sin(\alpha_{ij}) & \cos(\alpha_{ij}) & 0 \\ 0 & 0 & 0 & 1 \end{bmatrix}, \tag{2}$$

$$R_z(\theta_{ij}) = \begin{bmatrix} \cos(\theta_{ij}) & -\sin(\theta_{ij}) & 0 & 0 \\ \sin(\theta_{ij}) & \cos(\theta_{ij}) & 0 & 0 \\ 0 & 0 & 0 & 0 \\ 0 & 0 & 0 & 1 \end{bmatrix}, \tag{3}$$

$$T_x(h_{ij}) = \begin{bmatrix} 0 & 0 & 0 & h_{ij} \\ 0 & 0 & 0 & 0 \\ 0 & 0 & 0 & 0 \\ 0 & 0 & 0 & 1 \end{bmatrix}. \tag{4}$$

After multiplying them together, the transformation matrix turns out to be,

$$\begin{aligned} Q_{ij}(\theta_{ij}, \alpha_{ij}, h_{ij}) &= \begin{bmatrix} \cos(\theta_{ij}) & -\sin(\theta_{ij}) \cdot \cos(\alpha_{ij}) & \sin(\theta_{ij}) \cdot \sin(\alpha_{ij}) & h_{ij} \cdot \cos(\theta_{ij}) \\ \sin(\theta_{ij}) & \cos(\theta_{ij}) \cdot \cos(\alpha_{ij}) & -\cos(\theta_{ij}) \cdot \sin(\alpha_{ij}) & h_{ij} \cdot \sin(\theta_{ij}) \\ 0 & \sin(\alpha_{ij}) & \cos(\alpha_{ij}) & 0 \\ 0 & 0 & 0 & 1 \end{bmatrix} \\ &= \begin{bmatrix} R_{3\times 3}(\alpha_{ij}, \theta_{ij}) & T_{3\times 1}(\theta_{ij}, h_{ij}) \\ \mathbf{0}_{1\times 3} & 1 \end{bmatrix}. \end{aligned} \tag{5}$$

The closure condition of the MSTO structure can be expressed as,

$$Q_{12}Q_{23}Q_{34}Q_{41} = I. \tag{6}$$

1.3 Degree-4 MSTO structure with in-plane hinge-shift

The application of the in-plane hinge-shift technique involves translation along the z-axis of the hinges' coordinate systems. Therefore, the new transformation matrix based on the in-plane hinge-shift technique can be expressed as,

$$Q_{ij}(\theta_{ij}, \alpha_{ij}, h_{ij}, d_{ij}) = R_z(\theta_{ij})T_z(d_{ij})T_x(h_{ij})R_x(\alpha_{ij}), \tag{7}$$

where

$$T_x(h_{ij}) = \begin{bmatrix} 0 & 0 & 0 & 0 \\ 0 & 0 & 0 & 0 \\ 0 & 0 & 0 & d_{ij} \\ 0 & 0 & 0 & 1 \end{bmatrix}. \tag{8}$$

After multiplying matrix (3), (8), (4), and (2) in series, the transformation matrix is shown as follows,

$$\begin{aligned} Q_{ij}(\theta_{ij}, \alpha_{ij}, h_{ij}) &= \begin{bmatrix} \cos(\theta_{ij}) & -\sin(\theta_{ij})\cdot\cos(\alpha_{ij}) & \sin(\theta_{ij})\cdot\sin(\alpha_{ij}) & h_{ij}\cdot\cos(\theta_{ij}) \\ \sin(\theta_{ij}) & \cos(\theta_{ij})\cdot\cos(\alpha_{ij}) & -\cos(\theta_{ij})\cdot\sin(\alpha_{ij}) & h_{ij}\cdot\sin(\theta_{ij}) \\ 0 & \sin(\alpha_{ij}) & \cos(\alpha_{ij}) & d_{ij} \\ 0 & 0 & 0 & 1 \end{bmatrix} \\ &= \begin{bmatrix} R_{3\times3}(\alpha_{ij}, \theta_{ij}) & T_{3\times1}(\theta_{ij}, h_{ij}, d_{ij}) \\ \mathbf{0}_{1\times3} & 1 \end{bmatrix} \end{aligned} \tag{9}$$

Similarly, the closure condition of the MSTO structure with the in-plane hinge-shift technique can be expressed based on the chain rule as follows,

$$Q_{12}Q_{23}Q_{34}Q_{41} = I. \tag{10}$$

1.4 Degree-6 MSTO structure with hinge-inclination

The hinge-inclination technique means that the transformation among hinges involves the rotation along the y-axis of the hinges' coordinate system. Therefore, the transformation matrix can be expressed as follows,

$$Q_{ij}(\theta_{ij}, \alpha_{ij}, h_{ij}, d_{ij}, \beta_{ij}, \beta_{i'j}) = R_z(\theta_{ij})R_y(-\beta_{i'j})T_z(d_{ij})T_x(h_{ij})R_x(\alpha_{ij})R_z(\beta_{ij}), \tag{11}$$

where

$$i' = \begin{cases} i-1, & \text{if } i>1 \\ n, & \text{if } i=1 \end{cases}, \tag{12}$$

and

$$R_y(\beta_{ij}) = \begin{bmatrix} \cos(\beta_{ij}) & 0 & \sin(\beta_{ij}) & 0 \\ 0 & 1 & 0 & 0 \\ -\sin(\beta_{ij}) & 0 & \cos(\beta_{ij}) & 0 \\ 0 & 0 & 0 & 1 \end{bmatrix}. \tag{13}$$

The closure loop condition of the degree-6 MSTO structure can be expressed as,

$$Q_{12}Q_{23}Q_{34}Q_{45}Q_{56}Q_{61} = I. \tag{14}$$

2 Design details of MSTO design cases

2.1 Degree-4 MSTO structure with or without in-plane hinge-shift

The design parameters of MSTO structure with in-plane hinge-shift involve the hinge-shift parameters $\boldsymbol{d} = (d_{12}, d_{23}, \ldots, d_{n1})$, out-of-plane hinge-shift parameters $\boldsymbol{h} = (h_{12}, h_{23}, \ldots, h_{n1})$, and the rotation angle of the hinges at stable states $\boldsymbol{\Theta}^{\mathbf{sts}} = (\theta_{12}, \theta_{23}, \ldots, \theta_{n1}, \theta'_{12}, \theta'_{23}, \ldots, \theta'_{n1}, \ldots)$, shown as

$$P = \begin{bmatrix} \boldsymbol{h} \\ \boldsymbol{d} \\ \boldsymbol{\Theta}^{sts} \end{bmatrix}. \tag{15}$$

While the design parameters of the MSTO structure without the in-plane hinge-shift only contain the out-of-plane hinge-shift parameters, as shown in the following vector

$$P = \boldsymbol{h}. \tag{16}$$

To design an MSTO structure with or without the in-plane hinge-shift technique is to solve an optimization problem whose object function is the sum of stiffness based on the truss model at all the stable states. By maximizing the object function

$$\sum_{i=1}^{n} K_i, \tag{17}$$

under the following equality and inequality constraints.

For the degree-4 BSTO structure without in-plane hinge-shift, it can only be stable at a fully flat state $\Theta = (0, 0, 0, 0)$ and a fully folded state $\Theta = (\pi, \pi, \pi, \pi)$. Therefore, the equality closure constraint in eq. 6, only need to be satisfied in these two states

$$Q_{12}(0, \alpha_{12}, h_{12})Q_{23}(0, \alpha_{23}, h_{23})Q_{34}(0, \alpha_{34}, h_{34})Q_{41}(0, \alpha_{41}, h_{41}) = I, \tag{18}$$

and

$$Q_{12}(\pi, \alpha_{12}, h_{12})Q_{23}(\pi, \alpha_{23}, h_{23})Q_{34}(\pi, \alpha_{34}, h_{34})Q_{41}(\pi, \alpha_{41}, h_{41}) = I, \tag{19}$$

where $\boldsymbol{\alpha} = (\alpha_{12}, \alpha_{23}, \alpha_{34}, \alpha_{41})$ is set manually based on the origami pattern. In the example shown in Fig. 2(A), the pattern angles are $\boldsymbol{\alpha} = (\pi/4, \pi/2, 3\pi/4, \pi/2)$.

For the degree-4 BSTO structure with in-plane hinge-shift, the equality closure constraints shown in eq. 10 need to be satisfied at two stable states. As the zero-thickness origami pattern with a degree-4 vertex has one degree of freedom, we only need to provide one of the desired rotation angles at each stable state ${\theta_{12}}^{sts1}$ and ${\theta_{12}}^{sts2}$, shown as

$$Q_{12}({\theta_{12}}^{sts1}, \alpha_{12}, h_{12}, d_{12})Q_{23}(\theta_{23}, \alpha_{23}, h_{23}, d_{23})Q_{34}(\theta_{34}, \alpha_{34}, h_{34}, d_{34})Q_{41}(\theta_{41}, \alpha_{41}, h_{41}, d_{41}) = I, \tag{20}$$

and

$$Q_{12}({\theta_{12}}^{sts2}, \alpha_{12}, h_{12}, d_{12})Q_{23}(\theta'_{23}, \alpha_{23}, h_{23}, d_{23})Q_{34}(\theta'_{34}, \alpha_{34}, h_{34}, d_{34})Q_{41}(\theta'_{41}, \alpha_{41}, h_{41}, d_{41}) = I, \tag{21}$$

where $\boldsymbol{\alpha} = (\alpha_{12}, \alpha_{23}, \alpha_{34}, \alpha_{41})$ is set manually based on the origami pattern. In the example shown in Fig. 2(F), the pattern angles are $\boldsymbol{\alpha} = (\pi/3, 2\pi/3, 2\pi/3, \pi/3)$ and the desired rotation angles ${\theta_{12}}^{sts1}$ and ${\theta_{12}}^{sts2}$ are 0 and $\pi/2$.

The out-of-plane hinge-shift technique gives that, the 'valley' hinges need to lie on the top edges of the panel, while the 'mountain' hinges need to be at the bottom edges. Only the 1^{st} hinges of the two origami patterns shown in Fig. 2 are 'valley' hinges. Therefore, the inequality constraints related to the out-of-plane parameters are shown as follows,

$$\begin{bmatrix} h_{12} \\ -h_{41} \end{bmatrix} < \begin{bmatrix} 0 \\ 0 \end{bmatrix}. \tag{22}$$

Moreover, considering the folding direction of the 'mountain' and 'valley' hinges, the inequality constraints related to the hinges' rotation angles are shown as follows,

$$\begin{bmatrix} 0 \\ 0 \\ 0 \\ 0 \end{bmatrix} \leq \begin{bmatrix} -\theta_{23} \\ -\theta_{34} \\ -\theta_{41} \\ -\theta'_{23} \\ -\theta'_{34} \\ -\theta'_{41} \end{bmatrix} \leq \begin{bmatrix} \pi \\ \pi \\ \pi \\ \pi \\ \pi \\ \pi \end{bmatrix}. \tag{23}$$

For better convergence of the algorithm, the design parameters require upper and lower boundaries: for MSTO structure with in-plane hinge-shift,

$$\begin{bmatrix} \|h_{ij}\| \\ \|d_{ij}\| \end{bmatrix} < \begin{bmatrix} 1 \\ 0.1 \end{bmatrix}; \tag{24}$$

for MSTO structure without in-plane hinge-shift,

$$\|h_{ij}\| < 1. \tag{25}$$

2.2 Degree-6 MSTO with hinge-inclination

The design parameters of MSTO structure with in-plane hinge-shift and hinge-inclination involve the hinge-shift parameters $\boldsymbol{d} = (d_{12}, d_{23}, \ldots, d_{n1})$, out-of-plane hinge-shift parameters $\boldsymbol{h} = (h_{12}, h_{23}, \ldots, h_{n1})$, the rotation angle of the hinges at stable states $\boldsymbol{\Theta}^{\mathbf{sts}} = (\theta_{12}, \theta_{23}, \ldots, \theta_{n1}, \theta'_{12}, \theta'_{23}, \ldots, \theta'_{n1}, \ldots)$, and the hinge-inclination parameters $\boldsymbol{\beta} = (\beta_{12}, \beta_{23}, \ldots, \beta_{n1})$ shown as

$$P = \begin{bmatrix} \boldsymbol{h} \\ \boldsymbol{d} \\ \boldsymbol{\Theta}^{\mathbf{sts}} \\ \boldsymbol{\beta} \end{bmatrix}. \tag{26}$$

Similar to the bi-stable design in Sec. 2.1, the degree-6 MSTO structure with hinge-inclination should satisfy the closure constraints in eq. 14 at the three stable states,

$$Q_{12}(\theta_{12}, \alpha_{12}, h_{12}, d_{12}, \beta_{12}) \ldots Q_{61}(\theta_{61}, \alpha_{61}, h_{61}, d_{61}, \beta_{61}) = I, \tag{27}$$

$$Q_{12}(\theta'_{12}, \alpha_{12}, h_{12}, d_{12}, \beta_{12}) \ldots Q_{61}(\theta'_{61}, \alpha_{61}, h_{61}, d_{61}, \beta_{61}) = I, \tag{28}$$

$$Q_{12}(\theta''_{12}, \alpha_{12}, h_{12}, d_{12}, \beta_{12}) \ldots Q_{61}(\theta''_{61}, \alpha_{61}, h_{61}, d_{61}, \beta_{61}) = I, \tag{29}$$

where $\theta_{ij}, \theta'_{ij}, \theta''_{ij}$ denote the rotation angles of hinges at each stable state. Moreover, considering the rotation direction of the 'mountain' and 'valley' hinges, the inequality constraints of out-of-plane hinge-shift parameters and rotation angles can be set similarly to the Sec. 2.1. In the example shown in Fig. 3(D), the 3^{rd} and 5^{th} hinges are 'valley' hinges, while the others are 'mountain' hinges, therefore, the inequality constraints related to the folding directions are,

$$\begin{bmatrix} -h_{23} \\ h_{34} \\ -h_{45} \\ h_{56} \end{bmatrix} < \begin{bmatrix} 0 \\ 0 \\ 0 \\ 0 \end{bmatrix}, \tag{30}$$

and for each stable state,

$$\begin{bmatrix} 0 \\ 0 \\ 0 \\ 0 \\ 0 \\ 0 \end{bmatrix} \leq \begin{bmatrix} -\theta_{12} \\ -\theta_{23} \\ \theta_{34} \\ -\theta_{45} \\ \theta_{56} \\ -\theta_{61} \end{bmatrix} \leq \begin{bmatrix} \pi \\ \pi \\ \pi \\ \pi \\ \pi \\ \pi \end{bmatrix}. \tag{31}$$

However, after introducing the hinge-inclination, the relation among the rotation angles of hinges is no longer the same as its original origami pattern, we, instead, require the rotation angles to be close enough to that of the origami pattern,

$$\Theta = \begin{bmatrix} 0 \\ 0 \\ 0 \\ 0 \\ 0 \\ 0 \end{bmatrix}, \Theta' = \begin{bmatrix} -1.5708 \\ -0.9176 \\ 1.0204 \\ -2.8494 \\ 1.0204 \\ -0.9176 \end{bmatrix}, \Theta'' = \begin{bmatrix} \pi \\ \pi \\ \pi \\ \pi \\ \pi \\ \pi \end{bmatrix}. \tag{32}$$

Then, the inequality for the rotation angles of hinges can be expressed as follows,

$$\begin{bmatrix} \|\Theta^{sts1} - \Theta\| \\ \|\Theta^{sts2} - \Theta'\| \\ \|\Theta^{sts3} - \Theta''\| \end{bmatrix} \leq \begin{bmatrix} \epsilon \\ \epsilon \\ \epsilon \end{bmatrix}, \tag{33}$$

where $\epsilon = \pi/18$ in this example. Similar to Sec. 2.1, for better convergence, we set upper and lower boundaries for the design parameters,

$$\begin{bmatrix} \|h_{ij}\| \\ \|d_{ij}\| \\ \|\beta_{ij}\| \end{bmatrix} < \begin{bmatrix} 1 \\ 0.1 \\ \pi/36 \end{bmatrix}. \tag{34}$$

Therefore, the optimization problem for designing degree-6 MSTO structure is to maximize the sum of stiffness of stable states while subjecting to the equality and inequality constraints in eq. 27 - 34.

2.3 Multi-vertex degree-4 MSTO tessellation with in-plane hinge-shift

The Miura tessellation shown in Fig. 2, contains four degree-4 vertices with pattern angles $\boldsymbol{\alpha} = (\alpha_{12}, \alpha_{23}, \alpha_{34}, \alpha_{41})$. The objective function of this problem is the summation of the stiffness of each vertex at the stable states. For each vertex, there exist similar equality and inequality constraints as shown in eq. 20 - 24. For convenience, we take the absolute height of the hinges as the design parameters. Then the design parameters for one vertex can be written as,

$$P = \begin{bmatrix} \boldsymbol{H} \\ \boldsymbol{d} \\ \boldsymbol{\Theta^{sts}} \end{bmatrix}, \tag{35}$$

where the desired rotation angles ${\theta_{1,12}}^{sts1}$ and ${\theta_{1,12}}^{sts2}$ are 0 and $\pi/2$ in this example.

The relation between the out-of-plane hinge-shift parameters $\boldsymbol{h} = (h_{12}, h_{23}, h_{34}, h_{41})$ and the absolute height $\boldsymbol{H} = (H_1, H_2, H_3, H_4)$, can be

$$\begin{bmatrix} h_{12} \\ h_{23} \\ h_{34} \\ h_{41} \end{bmatrix} = \begin{bmatrix} -1 & 1 & 0 & 0 \\ 0 & -1 & 1 & 0 \\ 0 & 0 & -1 & 1 \\ 1 & 0 & 0 & -1 \end{bmatrix} \begin{bmatrix} H_1 \\ H_2 \\ H_3 \\ H_4 \end{bmatrix}. \tag{36}$$

Then the constraints for the coupled hinges' absolute heights and rotation angles can be shown as follows,

$$\begin{bmatrix} H_{3,1} - H_{1,2} \\ H_{4,2} - H_{4,3} \\ H_{3,3} - H_{1,4} \\ H_{4,4} - H_{4,1} \end{bmatrix} = \begin{bmatrix} 0 \\ 0 \\ 0 \\ 0 \end{bmatrix}, \tag{37}$$

$$\begin{bmatrix} \theta_{34,1} - \theta_{12,2} \\ \theta_{41,2} - \theta_{41,3} \\ \theta_{34,3} - \theta_{12,4} \\ \theta_{41,4} - \theta_{41,1} \end{bmatrix} = \begin{bmatrix} 0 \\ 0 \\ 0 \\ 0 \end{bmatrix}, \tag{38}$$

where $H_{i,k}$ and $\theta_{i,k}$ denote the absolute height and the rotation angles of the i^{th} hinge of vertex V_k, respectively. Additionally, because the four vertices (V_1, V_2, V_3, V_4) form a closed section in this pattern, an additional closed-loop constraint,

$$\begin{cases} (l_{3,1} - d_{3,1})z_{3,1} + (l_{4,2} - d_{4,2})z_{4,2} + (l_{3,3} - d_{3,3})z_{3,3} + (l_{4,4} - d_{4,4})z_{4,4} = 0 \\ h_{3,1}x_{3,1} + h_{4,2}x_{4,2} + h_{3,3}x_{3,3} + h_{4,4}x_{4,4} = 0 \end{cases}, \tag{39}$$

should be considered at the flat state during modeling.

3 Stiffness computation based on truss model

The truss model[42] used in this work follows the assumption that the elastic reconfiguration of structure is a combined result of in-plane deformation, the bending, and the folding of the panels. The mechanical behavior is described by the equilibrium equation, the compatibility equation, and the material properties respectively as:

$$\begin{cases} \mathbf{A} \cdot \mathbf{t} = \mathbf{f} \\ \mathbf{C} \cdot \mathbf{d} = \mathbf{e} \\ \mathbf{G} \cdot \mathbf{e} = \mathbf{t} \end{cases} \tag{40}$$

where $\mathbf{A}$ is the equilibrium matrix relating the internal bar tensions $\mathbf{t}$ to the nodal forces $\mathbf{f}$, $\mathbf{C}$ is the compatibility matrix that translates the nodal displacement vector $\mathbf{d}$ to the bar extensions $\mathbf{e}$, and axial bar stiffness is described by the diagonal matrix $\mathbf{G}$. The linear-elastic properties of the 4R structure are characterized by eigenvalue decomposing its compatibility matrix and analyzing the vector space[43]. However, of the primary interest here is the stiffness matrix, which provides a relation from the external forces $\mathbf{f}$ to the nodal displacement $\mathbf{d}$, and thus:

$$\mathbf{K} \cdot \mathbf{d} = \mathbf{f} \rightarrow \mathbf{K} = \mathbf{C}^{\mathrm{T}} \cdot \mathbf{G} \cdot \mathbf{C} \rightarrow \mathbf{K}\mathbf{v}_i = \lambda_i \mathbf{v}_i \tag{41}$$

The eigenvalues λ_i of the stiffness matrix represent the elastic energy at each reconfiguration mode $\mathbf{v_i}$ of the corresponding eigenmode[45]. Considering deformation of structures, the energy is required, and thus the lowest eigenvalue is able to act as a metric to evaluate the minimum energy as deformation. Specifically, to compute the stiffness of the MSTO structure with the truss model, we simplify the panel between the adjacent hinges with a tetrahedron whose vertices are the terminals of the hinges, as in Fig. S3. The edges of it are assumed to be elastic springs and the deformation of the panel during the folding process will turn into the extension and contraction of the springs. To express the relative position of the hinges' terminals in the coordinate system of the first hinge, we first set the origin of the coordinate system at the origin of the first hinge and the z-axis along the hinge. Then the coordinates of all the terminals can be expressed as follows,

$$O_i = Q_{1,i} O_1, \tag{42}$$

$$T_i = Q_{1,i} T_z(1) O_1, \tag{43}$$

$$O_1 = \begin{bmatrix} 0 \\ 0 \\ 0 \\ 1 \end{bmatrix}, \tag{44}$$

where the matrix $Q_{i,j}$ is the transformation matrix between the coordinate system of the i^{th} hinge and the 1^{st} hinge. It can be expressed with the multiplication of the transformation matrix (5), (9), and (11), shown as,

$$Q_{1,i} = Q_{12} \dots Q_{ki}. \tag{45}$$

4 Analysis of stiffness subject to designable parameters of MSTO structures

To study the influence of different parameters, like in-plane hinge-shift parameters on the stiffness of the stable states, we proposed two different methods including a computational method based on the truss model (Fig. S3) and an analytical method based on the closed-loop constraints of the structure's geometric properties. To show the proportion of the stiffness change caused by the design parameters, the results shown in Fig. S4(A, C, D, and F), are plotted with the relative stiffness K_{rel}. Here, we set the relative stiffness of the structures with the largest stiffness K_m as 1, then for any other structures, their relative stiffness will be $K_{rel} = K/K_m$.

4.1 Degree-4 MSTO structure without in-plane hinge-shift

For a degree-4 MSTO structure without in-plane hinge-shift, we consider three main influences, including its deviation from the over-constraint mechanism, which is,

$$dv^{\text{D4}}_{\text{pseudo}} = \sin(\alpha_{12}) h_{23} + \sin(\alpha_{41}) h_{34}, \tag{46}$$

the pattern angle α_{12} of the first panel, and the pattern angle α_{23} of the second pane. The computational results are shown in Fig. S4(A), the scale of the structure is constrained by requiring the out-of-plane hinge-shift parameter of the 1^{st} hinge h_{12} to be one. For the analytical solution, we open the close chain of the degree-4 vertex at the red hinge shown in Fig. S4(B) and turn it into a parallel moving hinge. Under this condition, the rotational motion of each hinge is identical to that of the corresponding over-constraint mechanism. The deformation caused by geometric violation will be expressed in the split distance of the open hinge, the distance will then be used to approximately analyze the influence of the design parameters.

The closure constraint for a degree-4 MSTO without in-plane hinge-shift shown in Eq. 6, can also be expressed as

$$\begin{aligned} &Q_{12} Q_{23} - Q_{41}^{-1} Q_{34}^{-1} \\ &= \begin{bmatrix} R_{3\times3}(\alpha,\theta) & T_{3\times1}(\alpha,\theta,h) \\ 0_{1\times3} & 1 \end{bmatrix} . \\ &= 0 \end{aligned} \tag{47}$$

For the degree-4 MSTO structure with hinges' rotation angles equal to θ_{ij} and θ'_{ij} at stable states, the closed-loop constraints of out-of-plane hinge-shift parameters h_{ij} can be formed with the translational matrix $T_{3\times1}$

at the stable states as shown below,

$$\begin{bmatrix} T_{3\times1} \\ T'_{3\times1} \end{bmatrix} = \begin{bmatrix} \cos(\theta_{12}) & \cos(\theta_{12})\cos(\theta_{23}) - \cos(\theta_{12})\sin(\theta_{12})\sin(\theta_{23}) & \cos(\theta_{41}) & 1 \\ \sin(\theta_{12}) & \cos(\theta_{12})\cos(\theta_{12}) + \cos(\theta_{12})\cos(\theta_{12})\sin(\theta_{23}) & -\cos(\theta_{41})\sin(\theta_{41}) & 0 \\ 0 & \sin(\theta_{12})\sin(\theta_{23}) & \sin(\theta_{41})\sin(\theta_{41}) & 0 \\ \cos(\theta'_{12}) & \cos(\theta'_{12})\cos(\theta'_{23}) - \cos(\theta'_{12})\sin(\theta'_{12})\sin(\theta'_{23}) & \cos(\theta'_{41}) & 1 \\ \sin(\theta'_{12}) & \cos(\theta'_{23})\cos(\theta'_{12}) + \cos(\theta'_{12})\cos(\theta'_{12})\sin(\theta'_{23}) & -\cos(\theta'_{41})\sin(\theta'_{41}) & 0 \\ 0 & \sin(\theta'_{12})\sin(\theta'_{23}) & \sin(\theta'_{41})\sin(\theta'_{41}) & 0 \end{bmatrix} \times \begin{bmatrix} h_{12} \\ h_{23} \\ h_{34} \\ h_{41} \end{bmatrix}. \tag{48}$$

When the structure is stable at the fully flat and fully folded states with hinges' rotation angles $\theta_{ij} = 0$, $\theta'_{ij} = \pi$, the closed-loop constraints for out-of-plane hinge-shift parameters can be derived as

$$\begin{bmatrix} T_{3\times1} \\ T'_{3\times1} \end{bmatrix} = \begin{bmatrix} 1 & 1 & 1 & 1 \\ 0 & 0 & 0 & 0 \\ 0 & 0 & 0 & 0 \\ -1 & 1 & -1 & 1 \\ 0 & 0 & 0 & 0 \\ 0 & 0 & 0 & 0 \end{bmatrix} \times \begin{bmatrix} h_{12} \\ h_{23} \\ h_{34} \\ h_{41} \end{bmatrix} \tag{49}$$

In order to study the energy change analytically of the bi-stable thick-origami structure with a single degree-4 vertex during the deformation process, one of the hinges can be assumed to be separated, and each of its terminals can be connected with a spring, as shown in Fig. S4(B). At the same time, it is assumed that the two sides of the separated hinges should keep parallel at all times during the transformation progress, so that the rotation of each hinge will still satisfy the Bennett linkage condition. Therefore, the energy change of the bi-stable thick-origami structure can be expressed by the separating distance between the terminals (elongation of the spring). Denote one of the coordinates of the origin of the first hinge as $O_1 = (0, 0, 0, 1)$ by a homogeneous vector, and based on the D-H parameters, the deformation energy during the transformation can be expressed as

$$E = \frac{1}{2}k\Delta d^2, \tag{50}$$

where

$$\Delta d = 2 \times \left|(Q_{12}Q_{23} - Q_{41}^{-1}Q_{34}^{-1})x_0\right|. \tag{51}$$

For a Bennett Linkage, the relation between hinges' rotation angles should satisfy

$$\frac{\tan(\frac{\theta_{12}}{2})}{\tan(\frac{\theta_{23}}{2})} = \frac{\sin(\frac{\alpha_{12}-\alpha_{23}}{2})}{\sin(\frac{\alpha_{12}+\alpha_{23}}{2})} = \frac{1}{m}, \theta_{12} = \theta_{34}, \theta_{41} = -\theta_{23}, \tag{52}$$

where

$$m = \frac{\sin(\frac{\alpha_{12}+\alpha_{23}}{2})}{\sin(\frac{\alpha_{12}-\alpha_{23}}{2})} = \frac{\tan(\frac{\alpha_{12}}{2}) + \tan(\frac{\alpha_{23}}{2})}{\tan(\frac{\alpha_{12}}{2}) - \tan(\frac{\alpha_{23}}{2})}. \tag{53}$$

Then, the sine and cosine of the hinges' rotation angles can be expressed as

$$\sin(\theta_{12}) = \frac{2\tan(\frac{\theta_{12}}{2})}{1+\tan^2(\frac{\theta_{12}}{2})}, \cos(\theta_{12}) = \frac{1-\tan^2(\frac{\theta_{12}}{2})}{1+\tan^2(\frac{\theta_{12}}{2})}; \tag{54}$$

$$\sin(\theta_{23}) = \frac{2m\tan(\frac{\theta_{12}}{2})}{1+m^2\tan^2(\frac{\theta_{12}}{2})}, \cos(\theta_{23}) = \frac{1-m^2\tan^2(\frac{\theta_{12}}{2})}{1+m^2\tan^2(\frac{\theta_{12}}{2})}. \tag{55}$$

According to Eq. 49, the compatibility constraints of out-of-plane hinge-shift parameters is

$$h_{12} + h_{23} + h_{34} + h_{41} = 0, h_{12} - h_{23} + h_{34} - h_{41} = 0. \tag{56}$$

Moreover, the flat-foldability of the origami pattern with a degree-4 vertex requires,

$$\alpha_{12} + \alpha_{34} = \alpha_{23} + \alpha_{41} = \pi \tag{57}$$

Substituting Eq. 54, Eq. 55, Eq. 56, and (57) into the deformation energy in Eq. 50, it turns out to be,

$$E \propto \Delta d^2 = \frac{16D^2(1+m^2+2m\cos(\alpha_{12}))\sin\left(\frac{\theta_{12}}{2}\right)^2}{1+m^2\tan\left(\frac{\theta_{12}}{2}\right)^2}, \tag{58}$$

where

$$D = \frac{h_{23}}{h_{12}} - \frac{\sin\alpha_{23}}{\sin\alpha_{12}} \tag{59}$$

denotes the deviation of the MSTO structure from its over-constraint mechanism counterpart.

Based on the deformation energy during the transformation process of the flat-foldable thick-origami model, its stiffness can be expressed as

$$K = \frac{d^2E}{d\theta_{12}^2} \propto \frac{d^2(\Delta d^2)}{d\theta_{12}^2}. \tag{60}$$

Substituting the 1^{st} hinge's rotation angle $\theta_{12}=0$, $\theta'_{12}=\pi$ into Eq. 60, the stiffness at the fully flat and fully folded state turns out to be,

$$K_0 = 4D^2(1+m^2+2m\cos(\alpha_{12})), \tag{61}$$

$$K_\pi = \frac{4D^2(1+m^2+2m\cos(\alpha_{12}))}{m^2}. \tag{62}$$

The stiffness of the degree-4 MSTO structure with pattern angles $\boldsymbol{\alpha}=(\pi/4,\pi/2,3\pi/4,\pi/2)$ at the fully flat stable state based on the analytical model is shown in Fig. 4(B). The difference between the analytical result and the computational result may be because of the different deformation processes during the transformation between the two stable states.

4.2 Degree-4 MSTO structure with in-plane hinge-shift

After introducing the in-plane hinge-shift technology to achieve intermediate stable states, we should further consider the influence of the scale of the hinge-shift parameter and the difference between stable states on the stiffness of the structure. Because the basis origami pattern is unchanged while changing the design parameters, the transformation between rotation angles θ_{12} and θ_{23} is constant, and the difference between stable states can be simplified to be $\|\theta_{12}-\theta'_{12}\|$. It's worth noting that the newly introduced parameter does not influence the previous effect. Similar to the computational analysis method for the MSTO structure without in-plane hinge-shift, the influence of the hinge-shift parameters and the difference between stable states can also be computed with the truss model, shown in Fig. 4(D). Analytical analysis can be derived similarly by the split distance at the open hinge, the red hinge in Fig. 4(E).

Similarly, the closure constraint for a degree-4 MSTO with in-plane hinge-shift shown in Eq. 10, can also be expressed as

$$\begin{aligned} & Q_{12}Q_{23} - Q_{41}^{-1}Q_{34}^{-1} \\ &= \begin{bmatrix} R_{3\times3}(\alpha,\theta) & T_{3\times1}(\alpha,\theta,h,d) \\ 0_{1\times3} & 1 \end{bmatrix}, \\ &= 0 \end{aligned} \tag{63}$$

where the out-of-plane hinge-shift parameter h_{ij} and the in-plane hinge-shift parameter d_{ij} are only related to the matrix $T_{3\times1}$.Therefore, for the MSTO structure with in-plane hinge-shift, the constraint matrix of the designable variables can be written as

$$\begin{bmatrix} T_{3\times1} \\ T'_{3\times1} \end{bmatrix} = C_{6\times8} \times \begin{bmatrix} h_{4\times1} \\ d_{4\times1} \end{bmatrix}, \tag{64}$$

where $h_{4\times1}$ and $d_{4\times1}$ are the out-of-plane hinge-shift parameters and the in-plane hinge-shift parameters.

Assuming the hinges' rotation angles at two stable states be $\theta=(\theta_{12},\theta_{23},\theta_{34},\theta_{41})$ and $\theta'=(\theta'_{12},\theta'_{23},\theta'_{34},\theta'_{41})$. Since the in-plane hinge-shift parameters do not affect the rotation matrix R3×3, the rotation angles at stable states still satisfy the same condition as shown in Eq. 54. Hence,

$$\sin(\theta_{12}) = \frac{2\tan(\frac{\theta_{12}}{2})}{1+\tan^2(\frac{\theta_{12}}{2})}, \cos(\theta_{12}) = \frac{1-\tan^2(\frac{\theta_{12}}{2})}{1+\tan^2(\frac{\theta_{12}}{2})}; \tag{65}$$

$$\sin(\theta_{23}) = \frac{2m\tan(\frac{\theta_{12}}{2})}{1+m^2\tan^2(\frac{\theta_{12}}{2})}, \cos(\theta_{23}) = \frac{1-m^2\tan^2(\frac{\theta_{12}}{2})}{1+m^2\tan^2(\frac{\theta_{12}}{2})}. \tag{66}$$

$$\sin(\theta'_{12}) = \frac{2\tan(\frac{\theta'_{12}}{2})}{1+\tan^2(\frac{\theta'_{12}}{2})}, \cos(\theta'_{12}) = \frac{1-\tan^2(\frac{\theta'_{12}}{2})}{1+\tan^2(\frac{\theta'_{12}}{2})}; \tag{67}$$

$$\sin(\theta'_{23}) = \frac{2m\tan(\frac{\theta'_{12}}{2})}{1+m^2\tan^2(\frac{\theta'_{12}}{2})}, \cos(\theta'_{23}) = \frac{1-m^2\tan^2(\frac{\theta'_{12}}{2})}{1+m^2\tan^2(\frac{\theta'_{12}}{2})}. \tag{68}$$

$$\theta_{12} = \theta_{34}, \theta_{41} = -\theta_{23}; \theta'_{12} = \theta'_{34}, \theta'_{41} = -\theta'_{23}, \tag{69}$$

where

$$m = \frac{\sin(\frac{\alpha_{12}+\alpha_{23}}{2})}{\sin(\frac{\alpha_{12}-\alpha_{23}}{2})} = \frac{\tan(\frac{\alpha_{12}}{2}) + tan(\frac{\alpha_{23}}{2})}{\tan(\frac{\alpha_{12}}{2}) - \tan(\frac{\alpha_{23}}{2})}. \tag{70}$$

From Eq. 64, the design parameters of a degree-4 MSTO structure with in-plane hinge-shift can be expressed as functions of h_{12} and d_{12}, as shown in the following equations,

$$\begin{bmatrix} h_{23} \\ h_{34} \\ h_{41} \\ d_{23} \\ d_{34} \\ d_{41} \end{bmatrix} = C'_{6\times2} \times \begin{bmatrix} -h_{12} \\ -d_{12} \end{bmatrix}, \tag{71}$$

where

$$C'_{6\times2} = \begin{bmatrix} -\frac{(1+c^2)(-1+m^2)}{c^2(-1+m)^2+(1+m)^2} & \frac{2cm(a+b)(-1+m^2)}{(-1+abm^2)[c^2(-1+m)^2+(1+m)^2]} \\ 1 & 0 \\ \frac{(1+c^2)(-1+m^2)}{c^2(-1+m)^2+(1+m)^2} & -\frac{2cm(a+b)(-1+m^2)}{(-1+abm^2)[c^2(-1+m)^2+(1+m)^2]} \\ 0 & \frac{m-abm}{-1+abm^2} \\ 0 & 1 \\ 0 & \frac{m-abm}{-1+abm^2} \end{bmatrix}, \tag{72}$$

$$a = \tan(\frac{\theta_{12}}{2}); b = \tan(\frac{\theta'_{12}}{2}); c = \tan(\frac{\alpha_{12}}{2}). \tag{73}$$

Similar to Eq. 50 and 51, the deformation energy of the structure is also related to the split distance of the hinge. By substituting Eq. 65 - 73 into Eq. 63, the deformation energy turns out to be,

$$E \propto \Delta d^2 = k'(\theta_{12}, \theta'_{12}, \alpha_{12}, m, \Theta_{12})d_{12}^2. \tag{74}$$

When $\Theta_{12} = \theta_{12}$ or θ'_{12}, $k' = 0$. Based on the description of deformation energy during transformation, the stiffness at the stable states of the model with in-plane hinge-shift parameters can be obtained as

$$K_\theta = \frac{d^2E_\theta}{d\Theta_{12}^2} = \frac{8(1+a^2)(a-b)^2c^2d_{12}^2m^2(m^2-1)^2}{(abm^2-1)^2(1+c^2)(1+a^2m^2)(c^2(m-1)^2+(m+1)^2)}, \tag{75}$$

$$K_{\theta'} = \frac{d^2E_{\theta'}}{d\Theta_{12}^2} = \frac{8(1+b^2)(a-b)^2c^2d_{12}^2m^2(m^2-1)^2}{(abm^2-1)^2(1+c^2)(1+a^2m^2)(c^2(m-1)^2+(m+1)^2)}. \tag{76}$$

The stiffness of the degree-4 MSTO structure with pattern angles $\boldsymbol{\alpha} = (\pi/4, \pi/2, 3\pi/4, \pi/2)$, one of the stable state $\theta_{12} = 0$, and out-of-plane hinge-shift parameter $h_{12} = 1$ based on the analytical model is shown in Fig. 4(F). The analytical results match well with the computational results.

5 Bi-material 3D printing approach for MSTO structures

The origami 3D model is made entirely of TPU (Thermoplastic polyurethanes), in which the thickness of the hinge between the panels is 0.4 (mm) and the width of the hinges is 0.75 (mm). The water-soluble material PVA (Polyvinyl Alcohol) is sometimes used as the support material. All the filaments are used as received from Polymaker (China).

The 3D model was designed and exported to STL files via SOLIDWORKS (V2021, Dassault Systèmes SOLIDWORKS Corp., USA). After that, the STL file was sliced with the layer thickness as 0.1 (mm) and the filling rate as 8 % in Ultimaker Cura software. The bed temperature during the printing was set to 60 (°C). The printing temperature for TPU material and PVA material were 220 (°C) and 200 (°C), respectively. The printing speed for TPU material and PVA material was set to 30 (mm/min) and 40 (mm/min), respectively. The PVA part can be completely dissolved in 60 (°C) water after printing.

6 FEM simulation approach for MSTO structures

The model of the thick-origami structure was solved in the commercial finite-element software COMSOL. We use the Multibody Dynamics module to perform a transient analysis of the stable state transformation process in thick-origami structures.

When importing files, we use the LiveLink for SOLIDWORKS interface, which allows us to import assembly files that have already been set up in SOLIDWORKS. The advantage of using this interface is that subsequent changes to the model can be updated directly.

After importing the model, select Form Assembly and Create Consistent Pair to facilitate the composition of the hinge joint. The material of the model is defined as an elastomer with a density of 350 kg/m3, Young's modulus of 6 MPa, and Poisson's ratio of 0.36. These data come from tests and Polymaker (China).

For each pair of boundaries that make up a hinge, define them in order as Rigid Attachments. When setting up a hinge joint, define its corresponding attachments, as Source and Destination. The Source of the next hinge should be on the same panel as the Destination of the previous hinge. For the last hinge of the loop, the Source should be the same as the first one. The center of the hinge is defined as the centroid of the junction edge between two panels. The model meshing is controlled by the physical field and the size is extremely fine.

In the module `Multibody Dynamics`, we can add fixed constraints to the boundaries, and assign motions or add driving forces to the hinge joints. Once the solution is complete, we can obtain the predefined variables, such as rotation angle, stress, strain, and elastic strain energy, during the sable state transformation process and perform a series of post-processing on them.

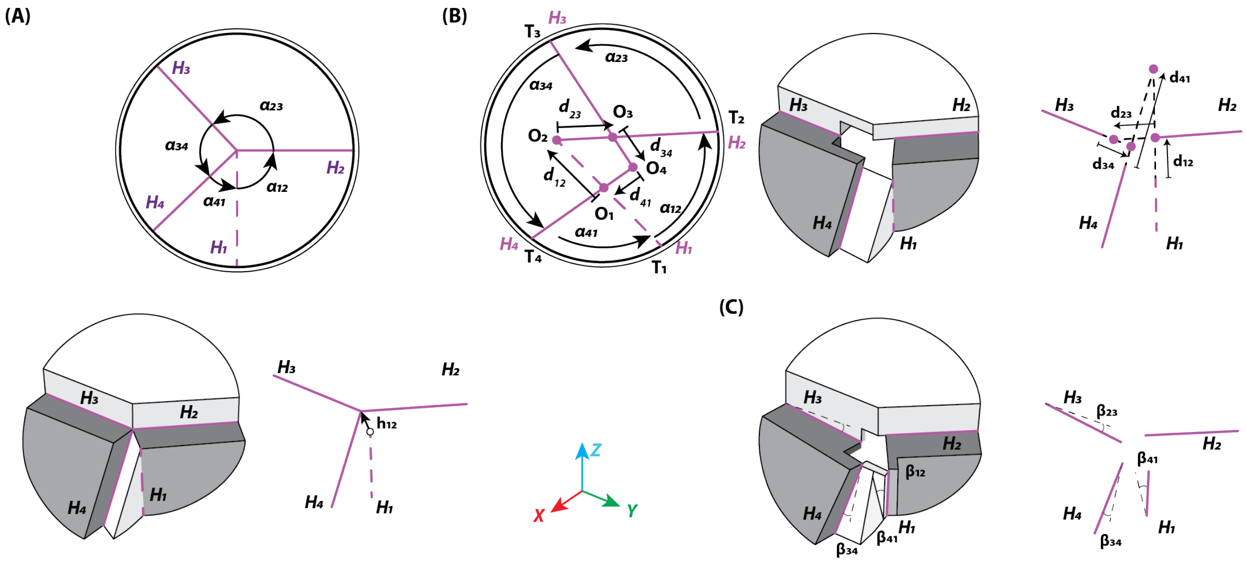

Fig. S1. Parameterization of MSTO structures. (**A**) MSTO structures with out-of-plane hinge shifting. (**B**)MSTO structures with out-of-plane and in-plane hinge shifting. (**C**) MSTO structures with out-of-plane and in-plane hinge-shift and hinge-inclination.

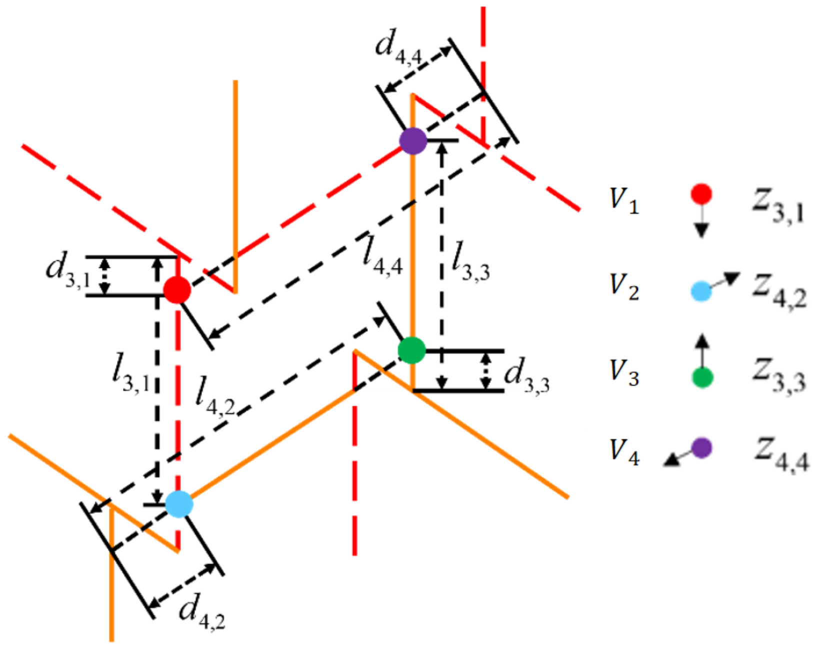

Fig. S2. Illustration of multi-vertex degree-4 MSTO tessellation with in-plane hinge-shift. The color circles denote the four vertices. Parameters $d_{i,k}$ and $l_{i,k}$ denote the in-plane hinge-shift parameter and the length of the i^{th} of the k^{th} vertex. Axis $z_{i,k}$ is the direction of the i^{th} of the k^{th} vertex.

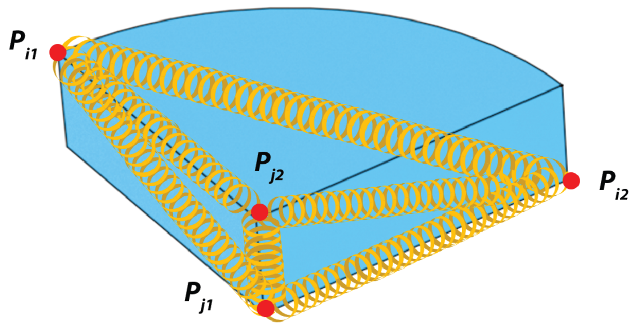

Fig. S3. Truss model of a thick panel. Illustration of the truss model of a thick panel and the panel between the hinges will be simplified to be a tetrahedron whose vertices are the terminal of the hinges $\mathrm{P}_{i1}, \mathrm{P}_{i2}, \mathrm{P}_{j1}, \mathrm{P}_{j2}$

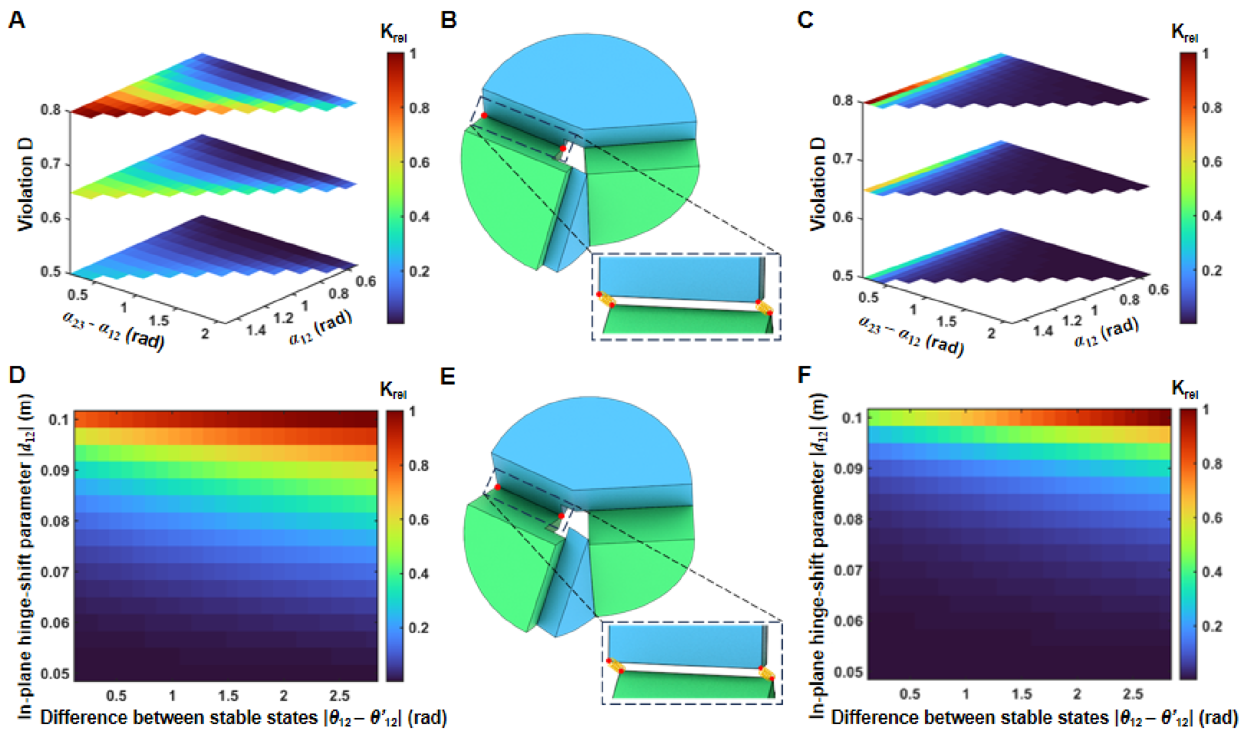

Fig. S4. Computational and analytical analysis of stiffness. (**A**) Computational result of the effect of the pattern angles and violation from the over-constraint mechanism on the stiffness of a flat-foldable bi-stable thick-origami structure with a degree-4 vertex. (**B**) Illustration of a flat-foldable bi-stable thick-origami structure with a parallel hinge (denoted with red dots). (**C**) Analytical result of the effect of the pattern angles and violation from the over-constraint mechanism on the stiffness of a flat-foldable bi-stable thick-origami structure with a degree-4 vertex. (**D**) Computational result of the effect of in-plane hinge-shift parameter and distance between stable states on a degree-4 vertex bi-stable thick-origami structure with an intermediate stable state ($\theta_{12} = 0$). (**E**) Illustration of an in-plane hinge-shift thick-origami structure with a parallel hinge (denoted with red dots). (**F**) Analytical result of the effect of in-plane hinge-shift parameter and distance between stable states on a degree-4 vertex bi-stable thick-origami structure with an intermediate stable state ($\theta_{12} = 0$).

Description of Additional Supplementary Files

1. Movies S1 to S7
   - **S1** : Video for the transformation process of flat-foldable bi-stable thick-origami structure with a single degree-4 vertex (experiment and simulation).
   - **S2** : Video for the transformation process of bi-stable thick-origami with the intermediate stable state (experiment and simulation).
   - **S3** : Video for the comparison of tri-stable thick-origami structure with a single degree-6 vertex before and after the introduction of hinge-inclination.
   - **S4** : Video for the transformation process of flat-foldable bi-stable Miura tessellation thick-origami structure (experiment and simulation).
   - **S5** : Video for the transformation process of bi-stable Miura tessellation thick-origami structure with the intermediate stable state (experiment and simulation).
   - **S6** : Video for the transformation process of the deployable tent and stairs.
   - **S7** : Video for the transformation process of the impulsive robotic gripper.
2. Data S1 to S2.
   - **S1** : Codes for MSTO structure design cases.
   - **S2** : Printable model of MSTO structure design cases.